ACCURACY ENHANCEMENT OF VISION METROLOGY THROUGH AUTOMATIC TARGET PLANE DETERMINATION

J.O. Otepka [a*], C.S. Fraser [b]

[a] Institute of Photogrammetry & Remote Sensing, Technical University of Vienna, Gusshausstrasse 27-29/E122, 1040 Vienna, Austria – jo@ipf.tuwien.ac.at
[b] Department of Geomatics, University of Melbourne, Victoria 3010, Australia – c.fraser@unimelb.edu.au

Commission V, WG V/1

Keywords: Vision Metrology, Targets, Surface, Automation, Algorithms, Precision, Close Range Photogrammetry

ABSTRACT:

In digital close-range photogrammetry, commonly referred to as vision metrology, circular targets are often used for high precision applications. The most common target type used consists of retro-reflective material, which provides a high contrast image with flash photography. The measurement of image coordinates of signalised targets continues to be a factor limiting the achievable accuracy of high-precision vision metrology systems. Mathematical algorithms are used to determine the centres of imaged targets in 2D space. These 2D centroids are then used in a triangulation process to calculate the target position in 3D space. This computational process assumes that the targets represent perfect 'points' in space. However, in practice target-thickness and target-diameter can adversely effect this assumption, leading to the introduction of systematic errors and to incorrect calculation of 3D position. The paper presents the development of a target plane determination process, which will serve to automatically correct for these errors. This will also lead to high accuracies within the bundle adjustment via an improved mathematical model.

1. INTRODUCTION

Nowadays, vision metrology (VM) is regularly used in large-scale industrial manufacturing and precision engineering. The flexibility of the vision-based concept, combined with new developments such as high-resolution digital cameras and new computational models, has made digital close-range photogrammetry a highly-automated, high-precision three-dimensional (3D) coordinate measurement technology.

VM strategies employ triangulation to determine 3D object point coordinates. To achieve accuracy to a few parts per million, special targets are used to mark points of interest. Various investigations have shown that circular targets deliver the most satisfying results regarding accuracy and automated centroid recognition and mensuration. For such targets, retro-reflective material is widely used because on-axis illumination of these targets returns many times more light than a normal textured surface. This results in high contrast images, which are a key requirement for high precision in digital close-range photogrammetry.

The perspective properties of circular targets are such that a circle viewed from directions other than normal to the target surface will appear as an ellipse or in general as a conic section, as indicated in Figure 1. Parabolic and hyperbolic curves appear only if the circle touches or intersects the "vanishing plane" (the plane parallel to the image plane, which includes the projection centre). Because of the typically small size of targets employed and the limited field of view of the measuring devices, it is unlikely that these circular targets will appear as parabolic or hyperbolic curves. Therefore, only elliptical images are considered in the following.

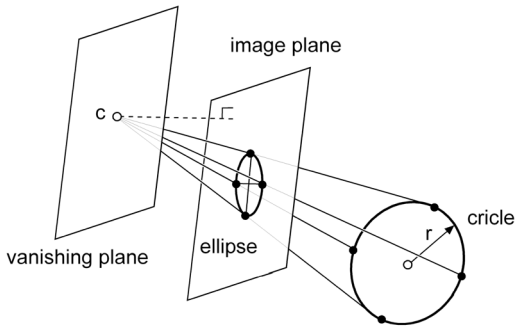

Figure 1. Perspective view of circle.

VM systems use centroiding algorithms to compute the centres of each ellipse, these centroids becoming the actual observations for the triangulation process. However, it is well known that the centre of a circle does not project onto the centre of the ellipse, which thus introduces a systematic error in any triangulation process. There are two reasons why this error is universally ignored in today's VM systems. First, the effect is small, especially in case of small targets (Dold, 1996; Ahn et. al, 1997). Second, to date there has been no practical method to automatically determine the target plane, which is a basic requirement for the correction of this error.

This paper presents an automatic target plane determination process which is applicable to any VM network using circular targets. As will be pointed out, ultra-precise surveys should benefit from the developed process because the systematic eccentricity error can be corrected, which will result in higher obtainable accuracy. However, even medium to high-precision applications can employ the target plane information to automatically compensate for target thickness in the case of

* Corresponding author

surface inspections, for example in the measurement of antenna reflectors or moulded components.

The target plane determination process was implemented and evaluated in *Australis*, a photogrammetric software package for off-line VM (Fraser & Edmundson, 2000; Photometrix, 2004).

2. TARGET PLANE DETERMINATION

The proposed target plane determination process can be subdivided into two stages. First the ellipse parameters of the circular target are computed in each image. In the next stage the actual elements of the circular target (target plane normal and radius) are determined using the computed ellipse information and the exterior orientation (EO) of the images. Considering mathematical rigor, this stage should be performed inside the bundle adjustment since object points and the EO of the images are correlated (within the bundle). However, this fact may be neglected because the eccentricity error has only a very small effect on the parameters of the bundle adjustment. Hence, it is justified to compute the target elements only once when the bundle is near convergence. Then the final iterations are computed considering the eccentricity corrections.

In the following, knowledge of least-squares formulations in bundle adjustment is assumed and therefore only the fundamental observation equations for the adjustment models are derived.

2.1 Ellipse Parameter Determination by 2D Gaussian Distribution Fitting

The determination of the ellipse parameters is a delicate problem since targets are typically only a few pixels in diameter (see Figure 2). State-of-the-art VM systems only determine the centre of the imaged target, mostly via by the well-known intensity-weighted centroiding approach:

$$\begin{pmatrix} x_0 \\ y_0 \end{pmatrix} = \frac{\sum_{i=1}^{n}\sum_{j=1}^{m} g_{ij}\begin{pmatrix} x_{ij} \\ y_{ij} \end{pmatrix}}{\sum_{i=1}^{n}\sum_{j=1}^{m} g_{ij}} \tag{1}$$

Here, x_0, y_0 are the centroid coordinates, x_{ij}, y_{ij} are the pixel coordinates and g_{ij} are the grey values within a window of dimension n x m. It should be mentioned, that a careful thresholding process needs to be performed before the actual centroiding, to remove disturbing background noise. Equation 1 points out clearly that as much pixel information as possible is used to compute the target centre. This consideration is also accounted for in the determination process for the ellipse parameters.

The idea of using the 2D Gaussian distribution to find the centre of gravity of a 2D object can be found in literature quite often. However, a visual analysis of the Gaussian distribution (bell curve) and intensity images of real targets (Figure 2) proves that the Gaussian distribution fits well to small targets only. Bigger targets have an intensity plateau, which cannot be described by the Gaussian distribution.

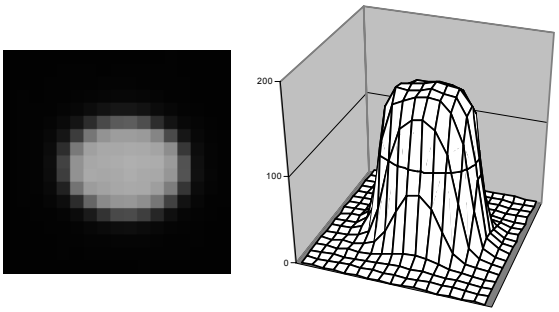

Figure 2: Typical target image in VM and its intensity image.

As it turns out, the cumulative Gaussian distribution (CGD) is an ideal base function (Figure 3) for the designed target function, which allows a description of targets with the aforementioned intensity plateau.

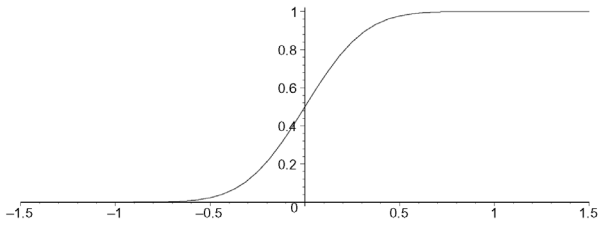

Figure 3: Cumulative Gaussian distribution (CGD).

The CGD is defined by

$$\Omega(x) = c\int_{-\infty}^{x} \mathrm{G}(x)dx = \frac{1}{\sqrt{2\pi\sigma^2}}\int_{-\infty}^{x} e^{-\frac{(x-\mu)^2}{2\sigma^2}}dx = \frac{1}{2}\,\mathrm{erf}\left(\frac{(x-\mu)}{\sqrt{2}\sigma}\right) + \frac{1}{2} \tag{2}$$

where G(x) is the Gaussian distribution, σ is the corresponding standard deviation and μ the expectation. Substituting x by $-(\bar{x}^{-2} - 1)$ in Equation 2 leads to the 1D function shown in Figure 4. The next step is to substitute x by an implicit ellipse equation, which results in the sought-after 2D function T.

$$\begin{pmatrix} \bar{x} \\ \bar{y} \end{pmatrix} = \begin{pmatrix} \cos\phi & \sin\phi \\ -\sin\phi & \cos\phi \end{pmatrix}\begin{pmatrix} x - c_x \\ y - c_y \end{pmatrix} \tag{3}$$

$$\mathrm{E} = \frac{\bar{x}^{-2}}{a^2} + \frac{\bar{y}^{-2}}{b^2} - 1 \tag{4}$$

$$\mathrm{T}(s, \beta, c_x, c_y, a, b, \phi, \sigma, \mu = 0) = s \cdot \Omega(-\mathrm{E}) + \beta \tag{5}$$

Equation 3 describes a transformation, the use of which within the implicit ellipse equation 4 allows the interpretation of c_x and c_y as the centre of the ellipse and ϕ as the bearing of the semi major axis.

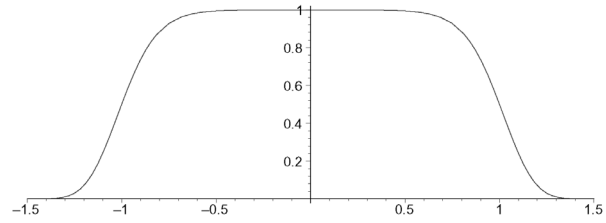

Figure 4: Target function derived from the CGD.

Formula 5 describes, for the adjustment used, the best-fit equation where s defines a scale factor (Ω can only provide values between 0 and 1) and β is background noise. By modelling the background, the thresholding process needed for the intensity-weighted centroiding can be avoided.

Figures 5 and 6 afford a better understanding of the parameters of the target function T; they show graphs using different parameter sets for T. Especially noteworthy is the last parameter σ (0.1 and 0.3), which defines the sharpness of the target signal. For completeness, it should be mentioned that horizontal sections of T are ellipses.

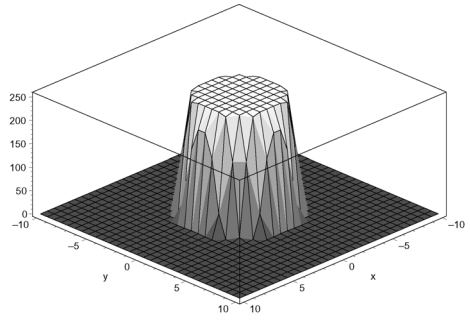

Figure 5: Graph of T(255, 0, 0 , 0, 4, 4, 0, 0.1).

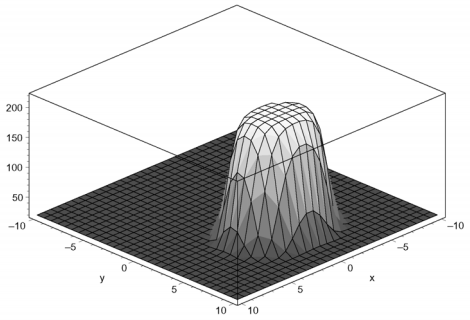

Figure 6: Graph of T(200, 20, 0 , 4, 4, 3, 0, 0.3).

The function T turns out to be an ideal target function to perform a best-fit adjustment where the grey values of the pixels are taken as observations and the parameters of T as unknowns. As can be seen, this estimation process is non-linear and therefore partial derivatives of T with respect to each parameter are required. Since the derivations are straight forward, only the final equations are presented here. The partial derivative with respect to the ellipse parameters (Equations 6-8) contain only the Gaussian distribution G itself since the integral within the CGD Ω and the derivation cancel each other out.

$$\frac{\partial \mathrm{T}}{\partial c_x} = 2s \cdot c \cdot \sigma \cdot \mathrm{G}(-\mathrm{E})\left(\frac{\bar{x}\cos\phi}{a^2} - \frac{\bar{y}\sin\phi}{b^2}\right)$$
$$\frac{\partial \mathrm{T}}{\partial c_y} = 2s \cdot c \cdot \sigma \cdot \mathrm{G}(-\mathrm{E})\left(\frac{\bar{x}\sin\phi}{a^2} + \frac{\bar{y}\cos\phi}{b^2}\right) \qquad (6)$$

$$\frac{\partial \mathrm{T}}{\partial a} = 2s \cdot c \cdot \sigma \cdot \mathrm{G}(-\mathrm{E})\left(\frac{\overline{x^2}}{a^3}\right)$$
$$\frac{\partial \mathrm{T}}{\partial b} = 2s \cdot c \cdot \sigma \cdot \mathrm{G}(-\mathrm{E})\left(\frac{\overline{y^2}}{b^3}\right) \qquad (7)$$

$$\frac{\partial \mathrm{T}}{\partial \phi} = 2s \cdot c \cdot \sigma \cdot \mathrm{G}(-\mathrm{E}) \cdot \overline{xy}\left(\frac{1}{b^2} - \frac{1}{a^2}\right) \qquad (8)$$

$$\frac{\partial \mathrm{T}}{\partial \sigma} = -E \cdot s \cdot \mathrm{G}(-\mathrm{E})$$
$$\frac{\partial \mathrm{T}}{\partial s} = \Omega(-\mathrm{E}) \qquad (9)$$
$$\frac{\partial \mathrm{T}}{\partial \beta} = 1$$

2.2 Target Plane Adjustment by Observing the Implicit Ellipse Parameter

Kager (1981) has shown that only two different circles in space with the same radius can project onto the same ellipse within the image. Hence, two images of the target have to exist to resolve this ambiguity. This is of no concern since resolution of such ambiguity is a fundamental requirement within photogrammetry. On the other hand, because of the small diameter of the ellipse, its elements (semi major and semi minor axes, and bearing) can only be determined with low accuracy. Consequently all ellipse images of one target have to be used to achieve the highest possible accuracy of the target plane. Therefore VM can offer ideal prerequisites since targets are generally imaged multiple times (>4).

The proposed target plane adjustment is performed for each target at the time of observing the implicit ellipse parameters of all images with known EO. To perform this, the mathematical connection between the circular target in object space and the ellipse parameters in image space has to be derived.

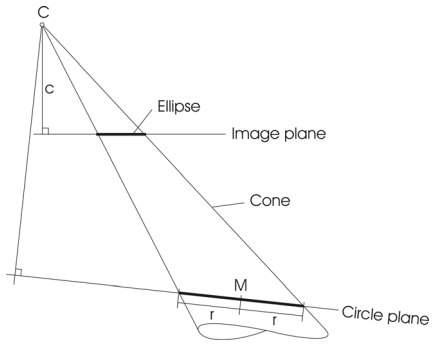

Figure 7: View cone which touches circular target.

An oblique cone is defined (Figure 7) which touches the circular target and the apex of the cone is positioned at the projection centre of the image. Then the cone is intersected with the image plane. If the resulting section figure can be presented in the same mathematical form as an implicit ellipse equation the problem is solved. That way, the ellipse parameters are represented by functions, which depend on the circle parameters and an adjustment of indirect observations can be performed.

In the object space, the cone can be described by

$$\mathbf{X} = \mathbf{C} + \lambda \cdot r \cdot \left(\cos\alpha \cdot \mathbf{e_1} + \sin\alpha \cdot \mathbf{e_2}\right) + \lambda \cdot (\mathbf{M} - \mathbf{C}) \qquad (10)$$

where **C** is the projection center, **e1** and **e2** are arbitrary orthogonal vectors within the circle plane, **M** is the midpoint of the circle and r the circle radius. Using the well known coplanarity equation

$$\begin{pmatrix} x \\ y \\ -c \end{pmatrix} = \mathbf{R} \cdot (\mathbf{X} - \mathbf{C}) = \begin{pmatrix} \mathbf{R}_1 \\ \mathbf{R}_2 \\ \mathbf{R}_3 \end{pmatrix} \cdot (\mathbf{X} - \mathbf{C}) \tag{11}$$

the cone can be transformed into image space by

$$\mathbf{x} = \lambda \cdot r \cdot \mathbf{R} \cdot (\cos\alpha \cdot \mathbf{e_1} + \sin\alpha \cdot \mathbf{e_2}) + \lambda \cdot \mathbf{R} \cdot (\mathbf{M} - \mathbf{C}) \tag{12}$$

The intersection of Equation 12 with the image plane is simple. The plane is defined by z = -c. Hence, λ can be obtained from

$$\lambda = -\frac{c}{\mathbf{R}_3 \cdot (r \cdot \cos\alpha \cdot \mathbf{e_1} + r \cdot \sin\alpha \cdot \mathbf{e_2} + \mathbf{M} - \mathbf{C})} \tag{13}$$

and the coordinates of the intersection figure follow as

$$\begin{aligned} x &= -c \frac{\mathbf{R}_1 \cdot (r \cdot \cos\alpha \cdot \mathbf{e_1} + r \cdot \sin\alpha \cdot \mathbf{e_2} + \mathbf{M} - \mathbf{C})}{\mathbf{R}_3 \cdot (r \cdot \cos\alpha \cdot \mathbf{e_1} + r \cdot \sin\alpha \cdot \mathbf{e_2} + \mathbf{M} - \mathbf{C})} = -c \frac{\mathbf{R}_1 \cdot \mathbf{v}}{\mathbf{R}_3 \cdot \mathbf{v}} \\ y &= -c \frac{\mathbf{R}_2 \cdot (r \cdot \cos\alpha \cdot \mathbf{e_1} + r \cdot \sin\alpha \cdot \mathbf{e_2} + \mathbf{M} - \mathbf{C})}{\mathbf{R}_3 \cdot (r \cdot \cos\alpha \cdot \mathbf{e_1} + r \cdot \sin\alpha \cdot \mathbf{e_2} + \mathbf{M} - \mathbf{C})} = -c \frac{\mathbf{R}_2 \cdot \mathbf{v}}{\mathbf{R}_3 \cdot \mathbf{v}} \end{aligned} \tag{14}$$

If Equations 14 can be transformed so that the parameter α is eliminated, the implicit form of the ellipse equation (15) is found. The derivation is lengthy and only the final form of the implicit parameter is presented here:

$$a \cdot x^2 + b \cdot xy + c \cdot y^2 + d \cdot x + e \cdot y - 1 = 0 \tag{15}$$

$$\begin{aligned} a &= \frac{r^2 \cdot {m_1}^2 - {n_{11}}^2 - {n_{21}}^2}{\overline{d}} \\ b &= 2\frac{r^2 \cdot m_1 \cdot m_2 - n_{11} \cdot n_{12} - n_{21} \cdot n_{22}}{\overline{d}} \\ c &= \frac{r^2 \cdot {m_2}^2 - {n_{12}}^2 - {n_{22}}^2}{\overline{d}} \\ d &= 2 \cdot c\frac{r^2 \cdot m_1 \cdot m_3 - n_{11} \cdot n_{13} - n_{21} \cdot n_{23}}{\overline{d}} \\ e &= 2 \cdot c\frac{r^2 \cdot m_2 \cdot m_3 - n_{12} \cdot n_{13} - n_{22} \cdot n_{23}}{\overline{d}} \end{aligned} \tag{16}$$

where the following substitutions have been used:

$$\begin{aligned} m_1 &= \mathbf{R_3} \cdot \mathbf{e_2} \cdot \mathbf{R_2} \cdot \mathbf{e_1} - \mathbf{R_3} \cdot \mathbf{e_1} \cdot \mathbf{R_2} \cdot \mathbf{e_2} \\ m_2 &= \mathbf{R_1} \cdot \mathbf{e_2} \cdot \mathbf{R_3} \cdot \mathbf{e_1} - \mathbf{R_1} \cdot \mathbf{e_1} \cdot \mathbf{R_3} \cdot \mathbf{e_2} \\ m_3 &= \mathbf{R_1} \cdot \mathbf{e_2} \cdot \mathbf{R_2} \cdot \mathbf{e_1} - \mathbf{R_1} \cdot \mathbf{e_1} \cdot \mathbf{R_2} \cdot \mathbf{e_2} \\ n_{11} &= \mathbf{R_3} \cdot \mathbf{e_1} \cdot \mathbf{R_2} \cdot (\mathbf{M} - \mathbf{C}) - \mathbf{R_2} \cdot \mathbf{e_1} \cdot \mathbf{R_3} \cdot (\mathbf{M} - \mathbf{C}) \\ n_{12} &= \mathbf{R_1} \cdot \mathbf{e_1} \cdot \mathbf{R_3} \cdot (\mathbf{M} - \mathbf{C}) - \mathbf{R_3} \cdot \mathbf{e_1} \cdot \mathbf{R_1} \cdot (\mathbf{M} - \mathbf{C}) \\ n_{13} &= \mathbf{R_1} \cdot \mathbf{e_1} \cdot \mathbf{R_2} \cdot (\mathbf{M} - \mathbf{C}) - \mathbf{R_2} \cdot \mathbf{e_1} \cdot \mathbf{R_1} \cdot (\mathbf{M} - \mathbf{C}) \\ n_{21} &= \mathbf{R_2} \cdot \mathbf{e_2} \cdot \mathbf{R_3} \cdot (\mathbf{M} - \mathbf{C}) - \mathbf{R_3} \cdot \mathbf{e_2} \cdot \mathbf{R_2} \cdot (\mathbf{M} - \mathbf{C}) \\ n_{22} &= \mathbf{R_3} \cdot \mathbf{e_2} \cdot \mathbf{R_1} \cdot (\mathbf{M} - \mathbf{C}) - \mathbf{R_1} \cdot \mathbf{e_2} \cdot \mathbf{R_3} \cdot (\mathbf{M} - \mathbf{C}) \\ n_{23} &= \mathbf{R_2} \cdot \mathbf{e_2} \cdot \mathbf{R_1} \cdot (\mathbf{M} - \mathbf{C}) - \mathbf{R_1} \cdot \mathbf{e_2} \cdot \mathbf{R_2} \cdot (\mathbf{M} - \mathbf{C}) \\ \overline{d} &= c^2 \left({n_{13}}^2 + {n_{23}}^2 - r^2 \cdot {m_3}^2 \right) \end{aligned} \tag{17}$$

Thus, a description of the implicit ellipse parameters dependent on the circle parameters is found. For the target plane adjustment, linearisation with respect to the circle parameters (**M**, r, **e1** and **e2**) is required.

The chosen parameterisation of the circular target by midpoint **M**, radius r and circle plane vectors **e1** and **e2** consists of 10 elements. However, a circle in 3D can generally be described by 6 parameters, i.e. midpoint, radius and two rotation angles. Hence, the selected parameterisation has 4 degrees of freedom which have to be eliminated within the adjustment. One possibility is to introduce constraints. This was implemented in the developed process in *Australis*. There, the length of the vectors **e1** and **e2** was fixed to 1 and the orthogonality of **e1** and **e2** was secured. The final constraint prevented **e1** and **e2** from rotating within the plane of the circle.

Since the observations for this adjustment were created by a previous adjustment, the previously computed covariance information can be incorporated as well. Tests have shown that this is an absolute requirement for the computation of an accurate target plane since the implicit ellipse parameters have different scales and different accuracies (for introducing full variance/covariance matrices, see Mikhail et al. 1996).

Finally, it should be mentioned that the first adjustment delivers explicit ellipse parameters whereas the target plane adjustment takes implicit ellipse parameters. The required conversion of the parameters and of the covariance matrix is shown in the appendix.

3. QUALITY ANALYSIS OF THE TARGET PLANE DETERMINATION PROCESS

For the quality analysis of the developed target plane determination process an object with a precisely known surface shape was surveyed. The test field was placed on a calibration table which had a machine-levelled surface. The table was kindly made available by *Boeing Australia Limited* at a factory in Melbourne. The main aim of the test field was to investigate the target size effects and the accuracy of determining the target normal.

The targets of the test field were arranged in a 4 by 4 grid, and four different target sizes were used (3, 5, 6.4 and 9.4 mm). Thus, the test field consisted of 64 inspection targets and some additional system-required targets (Figure 8).

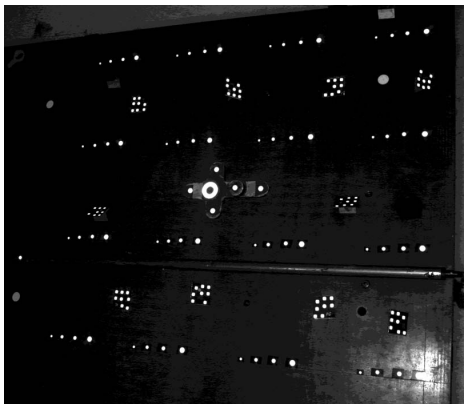

Figure 8: Test field on machine-levelled surface.

As expected, the bigger the target size the more accurately the target normal can be determined (Table 1). Whereas the results of the first three target classes are satisfactory, the target normals of the smallest target are undoubtedly not as good. These targets contain only very limited elliptical information (Figure 9) and therefore it is quite impressive how accurately the target normal can still be determined.

Average Target Diameter [pixel]	Average Angle Error [degrees]	Std. Error of Angle [degrees]
13.2	0.43	0.25
8.6	0.57	0.27
7.1	1.09	0.48
4.2	3.06	1.20

Table 1: Target normal statistic separated into the four target groups

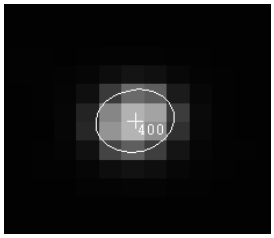

Figure 9: Target image of the smallest target group including the computed ellipse

VM is often used in surface inspections, where points on the surface are required. However, with the usage of targets the computed 3D coordinates are always positioned above the sought-after surface. With the knowledge of the target normal the corresponding point on the surface can be computed directly. This is a clear advantage for practical applications. Using a typical target thickness of 0.11 mm it can be estimated an angle error of 5 degrees results in a horizontal offset of only 10 μm (vertical offset less than 1 μm). This shows clearly that the achievable accuracy of the target normal even for small targets is good enough to compensate for target thickness.

4. THE ELLIPSE CENTRE ECCENTRICITY AND ITS DISTORTION EFFECTS ON THE BUNDLE ADJUSTMENT

Earlier investigations (Dold, 1996; Ahn et al., 1997) have studied the impact of the eccentricity error on a bundle adjustment. It was reported that in a free network adjustment with or without simultaneous camera calibration, the eccentricity error caused by moderately sized image targets is almost fully compensated for by changes in the exterior orientation parameters (and the principal distance) without affecting the other estimated parameters (Ahn et al., 1999).

Network simulations performed by the authors have shown good agreement with earlier findings, especially when employing test fields with little variation in the target normals. However, test fields with a significant range of target orientations and with medium to big-sized targets can show significant distortions within the triangulated object point coordinates. Such a simulated test field result is presented in the following.

The selected test field represents a sinus-shaped surface with the horizontal extent of 5 by 3 m (Figure 10). 16 images were artificially generated using a typical VM camera (c of 20 mm, resolution of 1500x1000 pixels). This resulted in an average target diameter of approximately 22 pixels within the images.

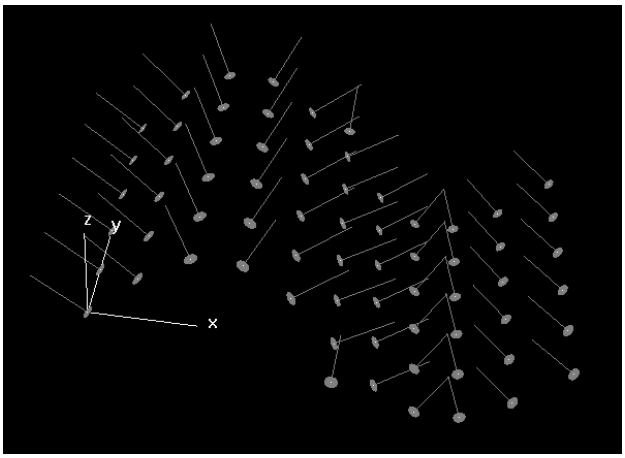

Figure 10: 3D view of sinus-shaped surface including target normals.

To investigate the eccentricity error, a free network adjustment using intensity-weighted target centroids was performed. Afterwards, the computed object coordinates were transformed into the original (error-free) coordinate reference frame. The resulting positional discrepancies are illustrated in Figure 11 and listed in Table 2.

	Average [mm]	Maximal [mm]
Discrepancies (transformation)	0.25	0.38
Object point sigma (bundle adjustment)	0.02	0.03

Table 2: Numerical results of bundle adjustment and the discrepancies within the original object coordinates.

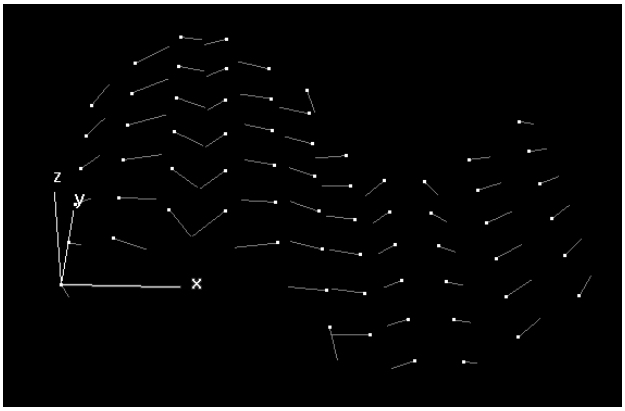

Figure 11: Discrepancy vectors between adjusted object coordinates and original coordinates.

From the results, interesting conclusions can be drawn. First, the eccentricity error can systematically distort the object point coordinates, this being visible in Figure 11. The amount of

distortion can clearly exceed the measurement accuracy of VM. The use of high quality digital equipment allows the achievement of typical triangulation accuracies of 1:100.000, which is about 0.05 mm in this case. However, the real accuracy of the presented network is about 0.25 mm for the object points (see Table 2).

Finally, a 'dangerous' effect for practical applications can be observed. Since the adjustment parameters compensate for the eccentricity error, the bundle adjustment estimates the accuracy of the object coordinates too optimistically (by factor 10 in this case), which may lead to misinterpretation, eg in deformation measurements.

Kager (1981) and Ahn et al. (1999) have developed two different correction formulae for the ellipse center eccentricity. Using Equations 16 and 17, the problem can solved via a third approach. First the implicit ellipse parameters of the imaged target circle are computed. This allows determination of the ellipse center coordinates (Equation 21). Using the image space target center and the ellipse center, the sough-after correction vector can be calculated. The equality of the three correction formulas was numerically proven by the authors.

5. DISCUSSION AND CONCLUSIONS

The presented target plane determination algorithm is a fully automated process which is suitable to any VM system which employs circular targets. The process has been implemented and evaluated within the *Australis* software system. As shown here, the algorithm can generate accurate target plane information, which will serve practical applications. The benefits are the correction of target thickness in the case of surface inspection and the general increased accuracy in ultra-precise surveys, since the observation equations of the bundle adjustment can be described more rigorously.

To date, one has always had to find a compromise between big (high centroiding accuracy) and small targets (small eccentricity error). The proposed method resolves this problem and allows use of big targets without the impact of eccentricity error.

Further research on real high-precision networks should further show that the accuracy of the object points can be increased by considering the eccentricity error. Since the improved accuracy is not 'visible' from internal measures within the bundle adjustment (as described in Section 4) ultra-precise reference (checkpoint) coordinates of object points are needed to verify the improved accuracy.

REFERENCES

Ahn, S.J., Warnecke, H.-J. and Kotowski, R., 1999. Systematic Geometric Image Measurement Errors of Circular Object Targets: Mathematical Formulation and Correction, *Photogrammetric Record*, 16(93), 485-502.

Ahn, S. J. and Kotowski, R., 1997. Geometric image measurement errors of circular object targets. *Optical 3-D Measurement Techniques IV* (Eds. A. Gruen and H. Kahmen). Herbert Wichmann Verlag, Heidelberg. 494 pages: 463–471.

Dold, J., 1996. Influence of large targets on the results of photogrammetric bundle adjustment. *International Archives of Photogrammetry and Remote Sensing*, 31(B5): 119–123.

Fraser, C.S., 1997. *Automation in Digital Close-Range Photogrammetry*, 1st Trans Tasman Surveyors Conference, Fryer J (ed), Proceedings of the 1st Trans Tasman Surveyors Conference, 1: 8.1 - 8.10. Newcastle, NSW: Institute of Surveyors, Australia.

Fraser, C.S. and Shao, J., 1997. *An Image Mensuration Strategy for Automated Vision Metrology*, Optical 3D Measurement Techniques IV, Heidelberg, Germany: Wichmann Verlag, 187-197.

Fraser, C. S. and Edmundson, K .L., 2000. Design and implementation of a computational processing system for off-line digital close range photogrammetry. *ISPRS Journal of Photogrammetry and Remote Sensing*, 55(1): 94-104.

Kager H., 1981, *Bündeltriangulation mit indirekt beobachteten Kreiszentren*. Geowissenschaftliche Mittelungen Heft 19, Institut für Photogrammetrie der Technischen Universität Wien.

Kraus, K., 1996, *Photogrammetrie*, Band 2: Verfeinerte Methoden und Anwednungen, Fred. Duemmlers Verlag.

Mikhail, Edward M. and Ackermann, F. (1996) *Observations and Least Squares*, IEP-A Dun-Donnelley.

Photometrix, 2004, Web site: http://www.photometrix.com.au (accessed 15 April 2004).

APPENDIX

In the following the conversion between explicit ellipse parameters and the implicit form (a general polynomial of the second degree, see Equation 15) is given. The parametric form of the ellipse equation can be described by

$$\begin{pmatrix} x \\ y \end{pmatrix} = \begin{pmatrix} M_x \\ M_y \end{pmatrix} + \begin{pmatrix} \cos\phi & \sin\phi \\ -\sin\phi & \cos\phi \end{pmatrix} \begin{pmatrix} A\cos\alpha \\ B\cos\alpha \end{pmatrix} \tag{18}$$

where M_x, M_y are the centre coordinates, ϕ is the bearing of the semi-major axis, and A and B are the semi major and semi minor axes of the ellipse.

The corresponding conversion to the implicit form follows as

$$\begin{aligned} \bar{a} &= \frac{\cos^2\phi}{B^2} + \frac{\sin^2\phi}{A^2} \\ \bar{b} &= 2\cdot\cos\phi\cdot\sin\phi\cdot\left(\frac{1}{B^2} - \frac{1}{A^2}\right) \\ \bar{c} &= \frac{\sin^2\phi}{B^2} + \frac{\cos^2\phi}{A^2} \\ \bar{f} &= 1 - M_x^{\,2}\cdot\bar{a} - M_x\cdot M_y\cdot\bar{b} - M_y^{\,2}\cdot\bar{c} \end{aligned} \tag{19}$$

$$a = \frac{\bar{a}}{\bar{f}} \qquad d = \frac{2 \cdot M_x \cdot \bar{a} - M_y \cdot \bar{b}}{\bar{f}}$$
$$b = \frac{\bar{b}}{\bar{f}} \qquad e = \frac{2 \cdot M_y \cdot \bar{c} - M_y \cdot \bar{b}}{\bar{f}} \tag{20}$$
$$c = \frac{\bar{c}}{\bar{f}}$$

The reverse conversion is given by

$$M_x = \frac{b \cdot e - 2 \cdot c \cdot d}{4 \cdot a \cdot c - b^2} \tag{21}$$
$$M_x = \frac{b \cdot d - 2 \cdot a \cdot e}{4 \cdot a \cdot c - b^2}$$

$$\phi = \frac{1}{2} \arctan \frac{b}{a - c} \tag{22}$$

$$A = \sqrt{\frac{1 - \frac{d}{2} M_x - \frac{e}{2} M_y}{c \cdot \cos^2\phi - b \cdot \sin\phi \cdot \cos\phi + a \cdot \sin^2\phi}} \tag{23}$$

$$B = \sqrt{\frac{1 - \frac{d}{2} M_x - \frac{e}{2} M_y}{a \cdot \cos^2\phi + b \cdot \sin\phi \cdot \cos\phi + c \cdot \sin^2\phi}}$$

Since the variance-covariance matrix Σ_I of the implicit parameters is needed for the target plane determination, error propagation can be used to transform the given variance-covariance matrix of the explicit parameters Σ_E by

$$\mathbf{\Sigma_I} = \mathbf{F_{E \to I}} \cdot \mathbf{\Sigma_E} \cdot \mathbf{F_{E \to I}^T} \tag{24}$$

where $\mathbf{F_{E \to I}}$ is define by

$$\mathbf{F_{E \to I}} = \begin{pmatrix} \frac{\partial a}{\partial M_x} & \frac{\partial a}{\partial M_y} & \frac{\partial a}{\partial \phi} & \frac{\partial a}{\partial A} & \frac{\partial a}{\partial B} \\ \frac{\partial b}{\partial M_x} & \frac{\partial b}{\partial M_y} & \frac{\partial b}{\partial \phi} & \frac{\partial b}{\partial A} & \frac{\partial b}{\partial B} \\ & & \vdots & & \\ \frac{\partial e}{\partial M_x} & \frac{\partial e}{\partial M_y} & \frac{\partial e}{\partial \phi} & \frac{\partial e}{\partial A} & \frac{\partial e}{\partial B} \end{pmatrix} \tag{25}$$